Transactions in Optics and Photonics
https://ojs.wiserpub.com/index.php/TOP/

Research Article

Thermoluminescence Properties of Ce, Dy Doped ZnB_2O_4 Phosphor

Kamlesh Thakkar[1†], Ravi Sharma[2*], Nameeta Brahme[1], D. P. Bisen[1], Anita Verma[3], Suman Sao[1]

[1] School of Studies in Physics and Astrophysics, Pt. Ravishankar Shukla University, Raipur (C.G), India
[2] Govt. Arts and Commerce Girls College Devendra Nagar, Raipur, C.G., India
[3] Dpeartment of Physics, Kalinga University, Naya Raipur (C.G), India
E-mail: artcommerce@gmail.com; kamleshthakkarap@gmail.com

Received: 15 September 2025; **Revised:** 24 November 2025; **Accepted:** 23 December 2025

Abstract: Samples of Ce^{3+} and Dy^{3+} doped Zinc Borate (ZnB_2O_4) phosphors were synthesized using the solid-state reaction method. Structural characterization was performed using X-Ray Diffraction (XRD), surface morphology was analyzed by Field-Emission Scanning Electron Microscopy (FESEM), and elemental composition was determined via Energy Dispersive Spectroscopy (EDS). The XRD pattern of the synthesized sample closely matches the JCPDS 39-1126 reference. Thermoluminescence (TL) analysis revealed that the samples doped with 2 mol% Ce^{3+} and Dy^{3+} exhibit the highest TL intensity. Upon irradiation of both samples with varying Ultraviolet (UV) exposure times, the maximum TL intensity was observed with a 15-minute UV dose. Trapping parameters were calculated using Chen's method, and the relationship between total TL intensity and UV dose, as well as the TL emission spectra, were also recorded.

Keywords: ZnB_2O_4, thermo luminescence, phosphors, X-Ray Diffraction (XRD), Field-Emission Scanning Electron Microscopy (FESEM)

1. Introduction

Fundamental and applied research in radiation detectors frequently utilizes rare-earth-doped phosphors. These doped materials are in high demand due to their applications in traffic signals and automobile brake lights. They also play a critical role in the clinical, personal, and environmental monitoring of ionizing radiation. When crystalline materials are exposed to highly ionizing radiation, they emit light upon thermal stimulation. According to band theory, irradiation of the Thermoluminescent (TL) material generates electron-hole pairs, and defects in the lattice create localized energy levels within the forbidden energy gap. These electron-hole pairs are trapped in these defects. Upon heating, the trapped electron-hole pairs are energized, enabling them to escape. The electrons can either be retrapped beyond the conduction or valence band, where they recombine with other electrons or holes. The locations where recombination occurs are called recombination centers. If radiative recombination takes place, these centers are known as luminescence centers. As a result, when the trapped holes are released by heat and recombine with trapped electrons, TL occurs. The number of electrons increases with temperature, leading to radiative or non-radiative emission [1]. A glow curve is a plot of emitted light intensity as a function of temperature during the TL process at a given heating rate. This curve may exhibit multiple peaks, each corresponding to an energy level within the material participating in the TL process. Changes in the position, shape, and intensity of these peaks reflect the characteristics of the material, impurities, and defects present [2]. The TL

DOI:

response varies with the concentration of rare-earth impurities and radiation dose, making it useful for dosimetry and geological dating [3]. Each glow peak is associated with the release of an electron from a specific trap level within the material's energy band. The TL studies of borate-based compounds are particularly interesting due to their near tissue equivalence, low cost, thermal stability, high sensitivity, low synthesis temperature, and ease of preparation [4–9].

Among the various borate materials, Zinc Borate (ZnB_2O_4) is notable for its low toxicity, cost-effectiveness, high luminescence efficiency, and wide band gap [10–12]. When doped with rare-earth ions, it demonstrates promising applications, such as in long-lasting phosphors for emerging lighting displays, flat-panel displays, and Light-Emitting Diodes (LEDs). Previous studies have extensively explored the dosimetric properties of rare-earth-doped zinc borates [13–17].

Despite these numerous applications, the activation mechanisms of rare-earth ions within the host lattice of zinc borate remain inadequately understood. It is generally believed that lattice defects are closely linked to and stabilized by the rare-earth impurities. The trapped charge carriers can migrate to the emission sites, thereby enhancing the efficiency of TL materials. This study focuses on TL measurements, providing an opportunity to investigate key properties such as glow curves, dose-response behaviors, luminescent intensity, and kinetic parameters of Ce- and Dy-doped zinc borate. The TL kinetic parameters were evaluated using the peak shape method. Despite the substantial body of TL research in the literature, very few studies have specifically examined Ce- and Dy-doped ZnB_2O_4 phosphors.

2. Experimental

We synthesized Zinc Borate (ZnB_2O_4) phosphors using the solid-state reaction method. The starting materials used for the synthesis included Analytical Reagent (AR)-grade ZnC, H_3BO_3, Ce_2O_3, and Dy_2O_3. A specific stoichiometric ratio of the raw materials was accurately weighed and mixed. The mixture was ground for 4 hours using a combination of water and acetone, then sintered at 850 °C in a furnace under atmospheric conditions. The sample was maintained at 850 °C for five hours, after which the furnace was turned off. The samples were allowed to cool naturally before being ground again to obtain a fine powder. TL measurements were performed using a Nucleonix TL 10091 Thermoluminescent Dosimeter (TLD) reader.

3. Result and discussions

ZnB_2O_4 crystals exhibit a three-dimensional layered structure with BO_4 tetrahedra at the corners. Figure 1 presents the X-Ray Diffraction (XRD) pattern of pure ZnB_2O_4 phosphor. The XRD data were recorded over the 2θ range of 100° to 700°. The X-ray diffraction measurements were conducted using a Bruker AXS D8 Advance powder diffractometer, employing a Cu-Kα radiation source at 40 kV with a wavelength of 1.540598 Å. The 2θ angle was measured with a step size of 0.04° and a count time of 1.5 s per step. The synthesis temperature of the phosphor was 850 °C. The obtained XRD patterns were compared with the reference data from JCPDS file No. 39-1126.

Due to the very low concentration of impurities, the volume of the impurity phase interacting with the X-ray beam may be insufficient to produce strong or consistent diffraction peaks. Rare earth ions, such as Ce^{3+} and Dy^{3+}, typically substitute for host ions in the crystal lattice. When the impurity ions are well-dispersed and present in low concentrations, they generally cause only a slight shift in the main host peaks due to minor lattice strain, rather than introducing entirely new peaks. As shown in Figure 1, the small amount (2%) of Ce^{3+} and Dy^{3+} ions does not significantly alter the XRD pattern of the pure ZnB_2O_4 sample. All samples exhibit single-phase diffraction patterns with no evidence of secondary phases. The dopant ions do not affect the crystal structure of ZnB_2O_4, which retains a body-centered cubic structure with a lattice parameter of $a = 7.473$ Å and space group Im_3m, similar to the undoped ZnB_2O_4 phosphor. The highest diffraction intensity for all samples was observed at the (2 1 1) plane, with a 2θ value of approximately 29.6°. The crystallite sizes of the samples were found to range from 5 to 10 micrometers.

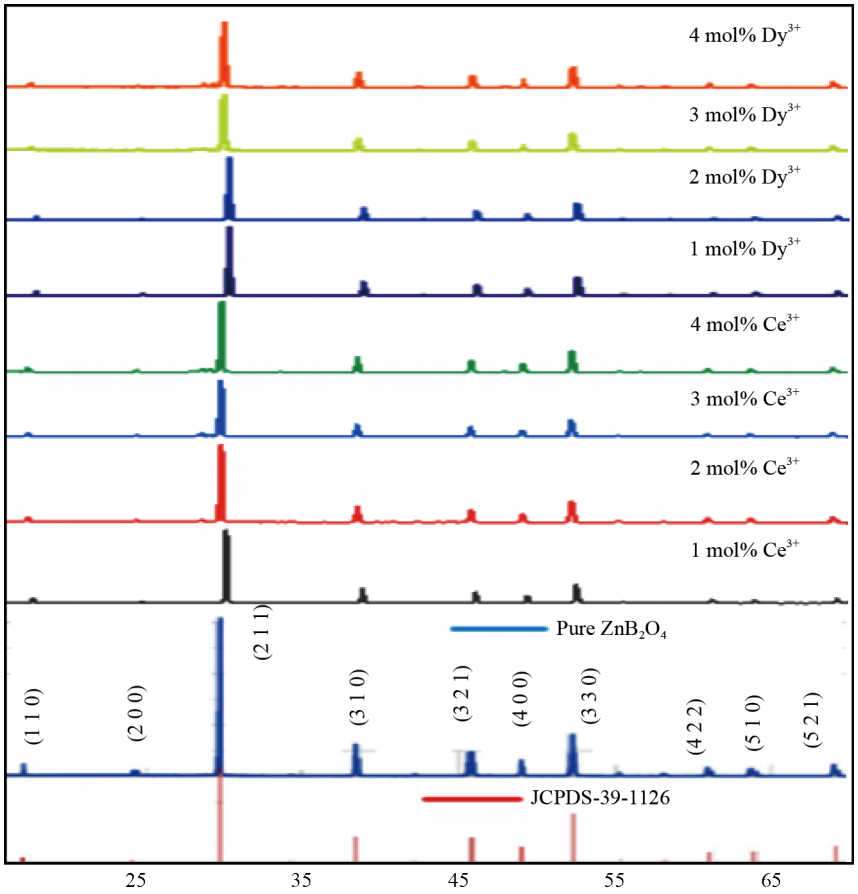

Figure 1. XRD of undoped, Ce and Dy doped ZnB_2O_4 and JCPDS file

4. Scanning electron microscopy and energy-dispersive X-ray spectroscopy analysis

In this study, a Carl Zeiss Ultra-High Resolution (UHR) FESEM Gemini Scanning Electron Microscope (SEM) 500, available at the Indian Institute of Technology, Bhilai (C.G.), India, was used to analyze FESEM images, Energy Dispersive Spectroscopy (EDS), and elemental mapping of the samples. The FESEM images reveal irregular, micro-sized crystallite structures, as shown in Figures 2a, c, and e. These images also indicate agglomeration in the sample. The particle size of the pure ZnB_2O_4 sample was found to be smaller than that of the doped samples. A flower-like structure is observed in the pure ZnB_2O_4 sample. In contrast, Figures 2c and 2e show larger, drier, clay-like structures in the doped samples. The Energy-Dispersive X-ray (EDX) spectra of the prepared undoped, Ce^{3+}-doped, and Dy^{3+}-doped ZnB_2O_4 samples confirm the incorporation of rare earth elements, as well as the elemental composition and stoichiometric ratio, as seen in Figures 2b, d, and f, respectively.

In the EDS analysis, the X-axis represents the energy of the detected X-rays, typically measured in kilo-electron Volts (keV). Each element in the sample emits characteristic X-rays at specific energy levels; thus, the position of the peaks along the X-axis is used for qualitative identification of the elements present. The Y-axis corresponds to the peak intensity, which represents the relative abundance or concentration of each element in the sample, and is used for quantitative analysis.

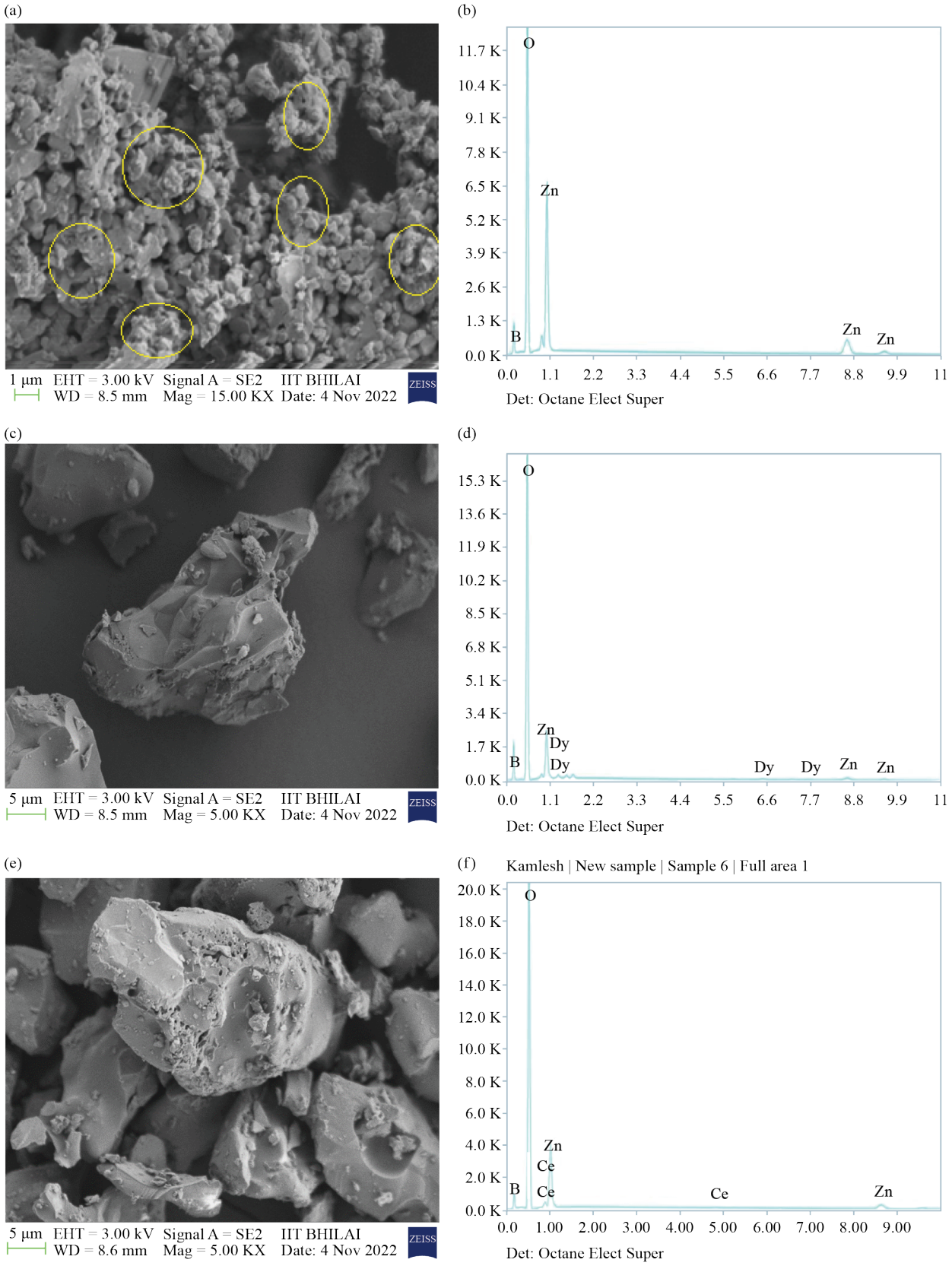

Figure 2. (a) FESEM image of pure ZnB_2O_4 phosphor; (b) EDX of pure ZnB_2O_4 phosphor; (c) FESEM of Dy doped ZnB_2O_4 phosphor; (d) EDX of Dy doped ZnB_2O_4 phosphor; (e) FESEM of Ce doped ZnB_2O_4 phosphor; (f) EDX of Ce doped ZnB_2O_4 phosphor

5. Thermoluminescence

The thermoluminescence process involves two main steps. First, the system transitions from an equilibrium state to a metastable state through the absorption of energy from ionizing radiation. Second, the system returns to the equilibrium state by releasing the absorbed energy in the form of light, typically through thermal stimulation. According to McKeever, the creation of defects occurs due to electronic excitation. Radiation-induced defects are localized electronic states that are occupied by a non-equilibrium concentration of electrons. According to energy band theory, between the conduction band and the valence band, two localized optical bands exist: one acts as a recombination center, and the other serves as a trap center. These localized optical bands arise due to the presence of impurities within the host lattice [18]. As a result of irradiation, both electrons and holes are generated. Electrons transition from the valence band to the conduction band and become trapped near the conduction band in what is referred to as an electron trap. The holes in the valence band occupy their corresponding traps, which are known as luminescence centers [19]. When heat is applied, the trapped electrons are released from the electron trap and recombine with the holes, as illustrated in Figure 3. This recombination process leads to the emission of photons.

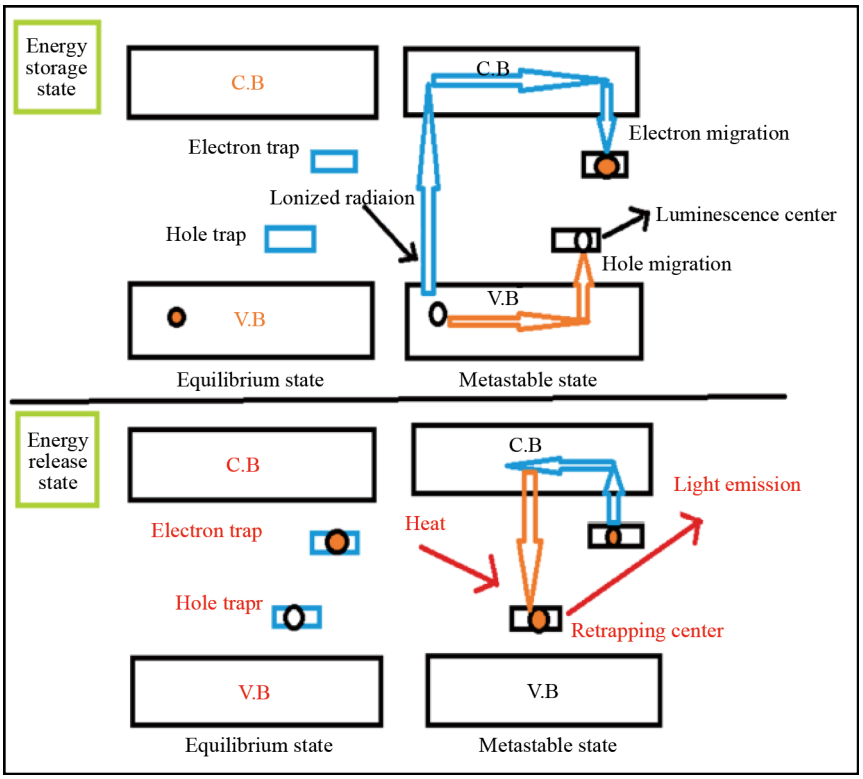

Figure 3. Basic mechanism of thermoluminescence

Thermoluminescence (TL) is a widely used technique for determining the trap level depth of materials. It has various applications across different fields, primarily due to its ability to measure the accumulated radiation doses in materials. The trap depth can be calculated by analyzing the kinetic parameters associated with TL. Several methods, including the initial rise method, heating rate method, isothermal method, and peak shape method, are commonly employed to analyze TL glow curve data. In this study, the deconvolution method is applied to determine the kinetic parameters of the prepared ZnB_2O_4 phosphor. The TL intensity of pure ZnB_2O_4 phosphor was measured using a fixed Heating Rate (HR) of 5 °C/s following a 15-minute Ultraviolet (UV) exposure.

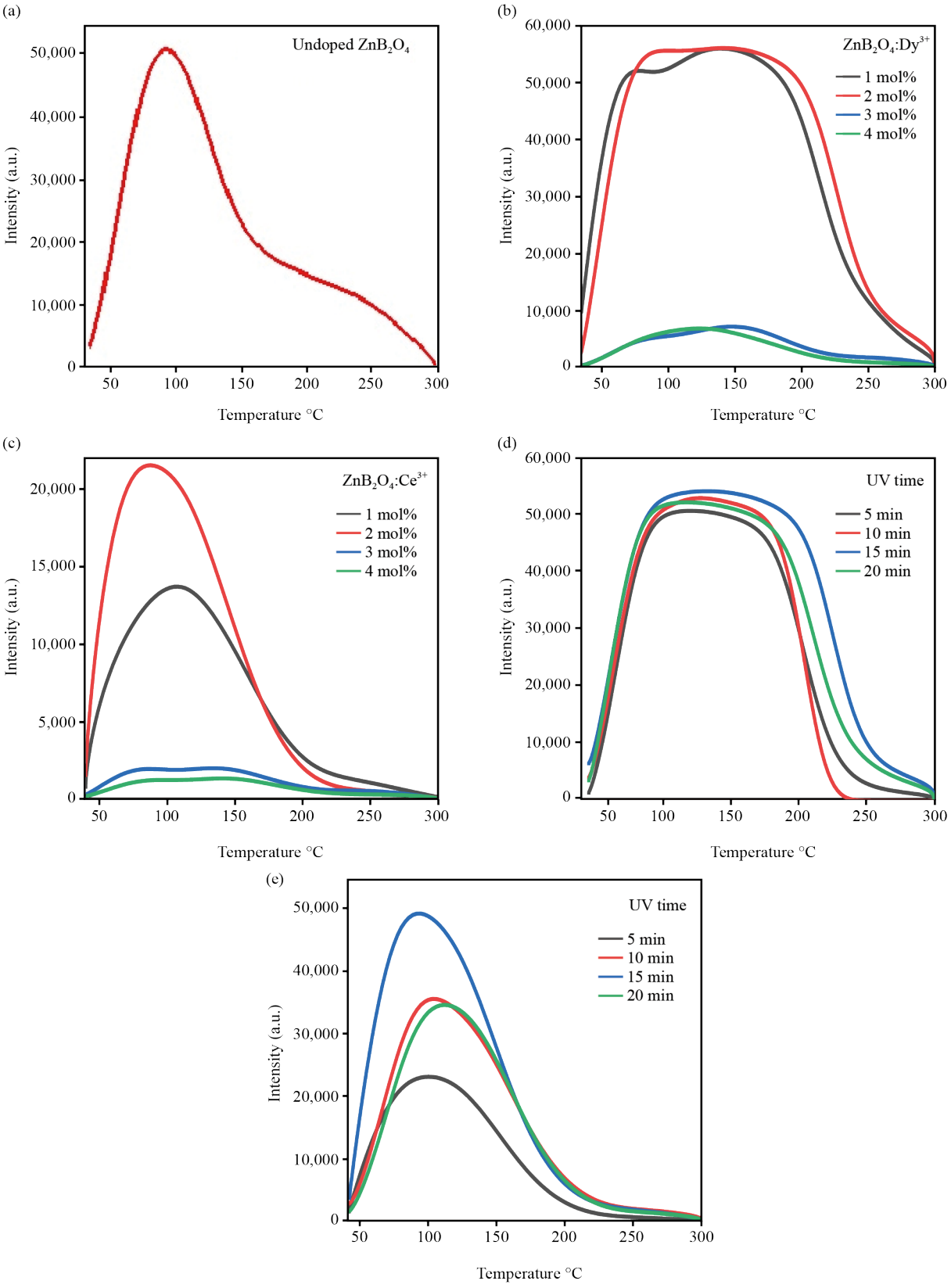

Figure 4. (a) TL glow curve of undoped ZnB_2O_4 phosphor; (b) TL glow curve of Dy^{3+} doped ZnB_2O_4 phosphor; (c) TL glow curve of Ce^{3+} doped ZnB_2O_4 phosphor; (d) Effect of UV exposure on Dy^{3+} doped ZnB_2O_4 phosphor; (e) Effect of UV exposure on Ce^{3+} doped ZnB_2O_4 phosphor

Figure 4a shows the TL intensity of pure ZnB_2O_4 phosphor as a function of temperature. It exhibits a broad peak centered at 92.5 °C, indicating strong TL intensity, with an additional shoulder observed at 237 °C. Figures 4b and 4c depict the variation in TL intensity for Dy^{3+}-doped and Ce^{3+}-doped ZnB_2O_4 samples, respectively. The molar percentage of dopants ranges from 1% to 4% for both impurities. The Dy^{3+}-doped sample presents a broad peak spanning from 60 °C to 190 °C. Notably, the TL intensity of the Dy^{3+}-doped sample is approximately twice that of the Ce^{3+}-doped sample.

The higher TL intensity observed in the Dy^{3+}-doped sample, compared to the Ce^{3+}-doped sample, is primarily attributed to its greater efficiency as a TL activator. Dy^{3+} serves as a primary luminescent center, contributing to both blue and yellow emissions, which are efficiently detected by standard detectors. In contrast, Ce^{3+} typically exhibits a broad emission band in the near-UV/blue region ($\sim$ 350-400 nm), which may be less effectively captured or coupled with the material's specific trap distribution. While Ce^{3+} is an efficient activator in Photoluminescence (PL), its performance in TL processes is less efficient.

Furthermore, the Ce^{3+}-doped sample displays a sharper peak compared to the Dy^{3+}-doped sample. The highest TL intensity for both samples occurs at a 2 mol% dopant concentration. All samples were exposed to UV light for 15 minutes. Beyond this concentration, TL intensity decreases due to non-radiative energy transfer, as activators can act as self-quenchers [20]. Therefore, 2 mol% Ce^{3+} and Dy^{3+} represent the optimal dopant concentrations for the synthesized samples.

Figures 4d and 4e illustrate the effect of UV dose on the TL properties of $ZnB_2O_4:Ce^{3+}$ and $ZnB_2O_4:Dy^{3+}$ phosphors. The UV dose was varied from 5 minutes to 20 minutes. The results clearly show that for $ZnB_2O_4:Ce^{3+}$, the integrated TL intensity initially increases with UV dose, reaching its maximum at 15 minutes, after which it begins to decrease. In contrast, for $ZnB_2O_4:Dy^{3+}$, the maximum TL intensity is observed at 15 minutes of UV irradiation. Exposure to UV light generates electron-hole pairs, with the RE^{3+} ions capturing the electrons and the holes being trapped at host-related centers. Upon heating, these holes are gradually untrapped at different temperatures according to the thermal stability of the material. The characteristic emission of RE^{3+} ions is observed as the ions decay to their ground state from the excited state. The increase in UV dose results in a higher concentration of active luminescent centers, leading to an enhancement in TL intensity. However, beyond a certain UV dose, only a limited number of RE ions are available for charge reduction, which may explain the observed saturation in TL intensity with further increases in UV exposure [21].

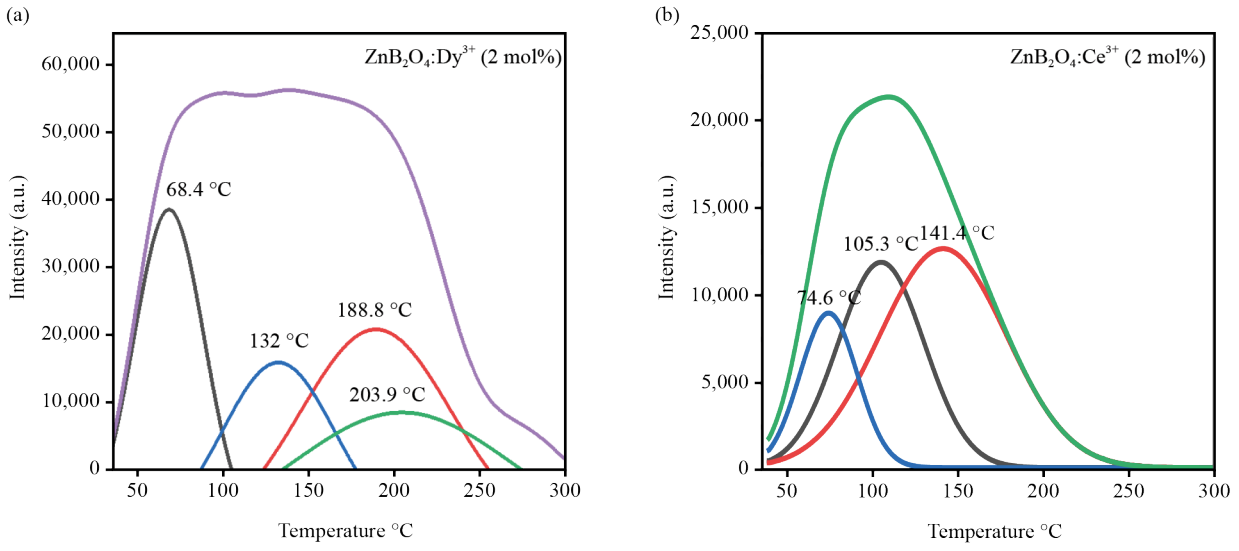

Figure 5. (a) Gaussian curve of Dy^{3+} doped ZnB_2O_4 phosphor; (b) Gaussian curve of Ce^{3+} doped ZnB_2O_4 phosphor

Figure 5a and 5b show the Gaussian curve fitting for the $ZnB_2O_4:Ce^{3+}$ and $ZnB_2O_4:Dy^{3+}$ phosphors, respectively. The superposition of multiple peaks results in a broad single glow peak. This broad peak was deconvoluted into three

distinct bands for $ZnB_2O_4:Ce^{3+}$ phosphor, located at 347.6 K, 378.3 K, and 414.1 K, and four bands for $ZnB_2O_4:Dy^{3+}$ phosphor, positioned at 341.4 K, 405.1 K, 461.8 K, and 476.9 K. The TL parameters for all deconvoluted peaks were calculated using Chen's method [22, 23]. The activation energy for $ZnB_2O_4:Ce^{3+}$ varies from 0.49 eV to 0.82 eV, and the frequency factor varies accordingly. Similarly, the activation energy for $ZnB_2O_4:Dy^{3+}$ ranges from 0.62 eV to 0.75 eV, with the corresponding frequency factor varying as well. These values are summarized in Tables 1 and 2.

Table 1. Trapping parameter of Ce^{3+} (2 mol%) doped ZnB_2O_4

Phosphor	Peak	T_m	τ	δ	ω	μ_g	E (ev)	S (s^{-1})
$ZnB_2O_4:Ce^{3+}$ (2%)	Peak 1	74.61	19.84	20.09	39.94	0.5	0.82	1.3×10^{13}
	Peak 2	105.29	29.63	30.08	59.71	0.5	0.63	3.1×10^{9}
	Peak 3	141.41	43.66	43.09	86.75	0.5	0.49	7.5×10^{6}

Table 2. Trapping parameter of Dy^{3+} (3 mol%) doped ZnB_2O_4

Phosphor	Peak	T_m	τ	δ	ω	μ_g	E (ev)	S (s^{-1})
$ZnB_2O_4:Dy^{3+}$ (3%)	Peak 1	68.42	20.66	20.37	41.03	0.5	0.75	1.9×10^{12}
	Peak 2	132.06	28.55	28.69	57.24	0.5	0.76	3.3×10^{10}
	Peak 3	188.87	39.87	40.02	79.89	0.5	0.69	3.0×10^{8}
	Peak 4	203.97	46.71	47.31	94.03	0.5	0.62	2.7×10^{7}

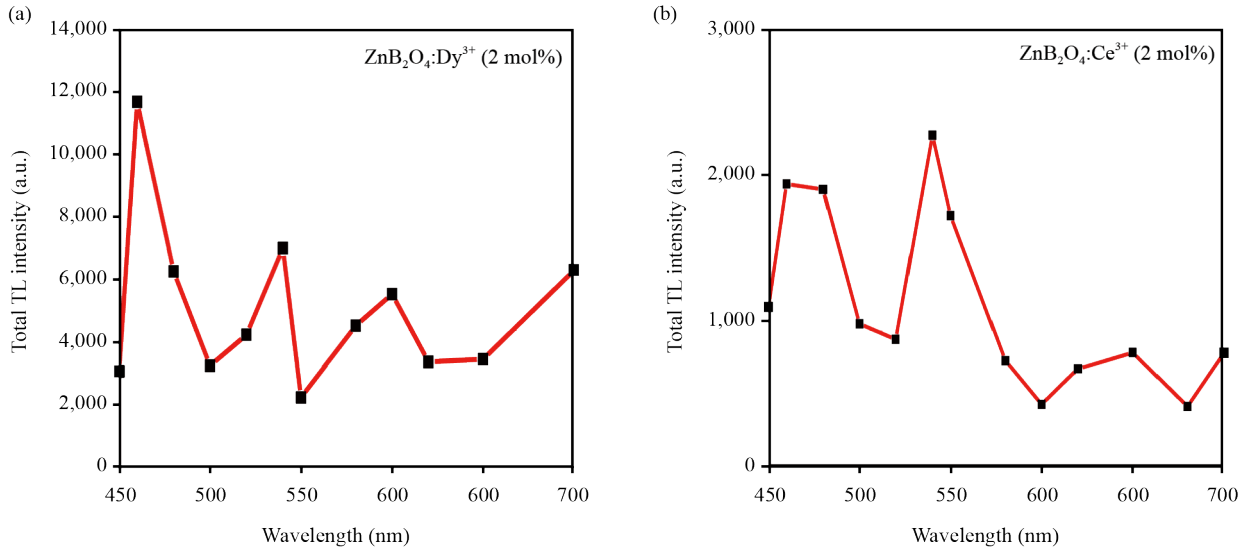

Figure 6. (a) TL emission spectra of Dy^{3+} doped ZnB_2O_4 phosphor; (b) TL emission spectra of Ce^{3+} doped ZnB_2O_4 phosphor

Figure 6a and Figure 6b show the TL spectra for $ZnB_2O_4:Ce^{3+}$ and $ZnB_2O_4:Dy^{3+}$ phosphors. TL spectra were recorded between wavelengths 450 and 700 nm using different interference filters.

Similar to the photoluminescence of Ce^{3+} doped phosphor, TL also has emission due to 4d-5f transitions. The peaks were recorded at 460 nm, 480 nm, 540 nm, and 650 nm, which confirms the emission due to 4d-5f transitions. In Dy^{3+}

doped ZnB_2O_4, we got maximum TL intensity at 460 nm out of three emission peaks at 460 nm, 540 nm, and 600 nm. This is due to the transitions of $4_{F_{9/2}}$ to $6_{H_{15/2}}$ [24].

6. Conclusions

Pure and Ce, Dy doped ZnB_2O_4 samples were synthesized by the solid state reaction method using Zinc Oxide (ZnO) and H_3BO_3 as starting materials. The crystallite sizes of the samples were found to be in the range 5-10 micrometers. Phase analysis confirms the body-centered cubic structure with $a = 7.473$ Ao and space group (Im_3m) as of undoped ZnB_2O_4 phosphor. The addition of rare earth does not bring any changes in the XRD pattern. The XRD image is also well matched with the reported JCPDS file no 39-1126. On irradiating both the samples with different UV exposure, 15-minute UV dose exhibited maximum TL intensity. The enhanced TL with an increase in UV dose is due to the rising number of traps. The maximum obtained TL was 2 mol% for both Ce^{3+} and Dy^{3+} doped samples. The average activation energy calculated was 0.65 eV, 0.69 eV, and the frequency factor was $\sim 7.87 \times 10^{10}$, $\sim 1.34 \times 10^{10}$ for Ce and Dy doped samples, respectively. The red emission peak at 680 nm is absent, whereas the blue emission at 460 nm and the yellow emission at 580 nm are observed in the TL spectra.

Data availability statements

The datasets generated during and/or analyzed during the current study are available from the corresponding author on reasonable request.

Author contributions

All authors contributed to the study conception and design. Material preparation, data collection and analysis were performed by Kamlesh Thakkar, Ravi Sharma, Nameeta Brahme, D. P. Bisen, Anita Verma and Suman Sao. The first draft of the manuscript was written by Ravi Sharma and all authors commented on previous versions of the manuscript. All authors read and approved the final manuscript.

Funding

The authors declare that no funds, grants, or other support were received during the preparation of this manuscript.

Conflict of interest

The authors declare that there is no conflict of interest.

References

[1] Thakkar K, Sharma R, Brahme N, Bisen DP, Verma A, Richhariya T. Luminescence studies of Sm^{3+} doped CdB_4O_7 phosphors. *Journal of Materials Science: Materials in Electronics*. 2023; 34: 1151. Available from: https://doi.org/10.1007/s10854-023-10520-9.

[2] Linganna K, Rao CS, Jayasankar CK. Optical properties and generation of white light in Dy^{3+}-doped lead phosphate glasses. *Journal of Quantitative Spectroscopy & Radiative Transfer*. 2013; 118: 40-48. Available from: https://doi.org/10.1016/j.jqsrt.2012.12.002.

[3] McKeever SWS. *Thermoluminescence of Solids*. Cambridge University Press; 1985

[4] Meijerink A, Blasse G, Glasbeek M. Photoluminescence, thermoluminescence and EPR studies on $Zn_4B_6O_{13}$. *Journal of Physics: Condensed Matter*. 1990; 2: 6303. Available from: https://doi.org/10.1088/0953-8984/2/29/008.

[5] Santiago M, Grasseli C, Caselli E, Lester M, Lavat A, Spano F. Thermoluminescence of SrB_4O_7:Dy. *Physica Status Solidi (A)*. 2001; 185(2): 285-289. Available from: https://doi.org/10.1002/1521-396X(200106)185:2<285::AID-PSSA285>3.0.CO;2-9.

[6] Zeng Q, Pei Z, Su Q, Lu S. Luminescence properties of Sm^{2+} in barium octaborates (BaB_8O_{13}:Sm^{2+}). *Journal of Luminescence*. 1999; 82(3): 241-249. Available from: https://doi.org/10.1016/S0022-2313(99)00041-1.

[7] Zeng Q, Pei Z, Wang S, Su Q, Lu S. Luminescent properties of divalent samarium-doped strontium hexaborate. *Chemistry of Materials*. 1999; 11: 605. Available from: https://doi.org/10.1021/cm980479i.

[8] Pei Z, Su Q, Zhang J. The valence change from RE^{3+} to RE^{2+} (RE Eu, Sm, Yb) in SrB_4O_7: RE prepared in air and the spectral properties of RE^{2+}. *Journal of Alloys and Compounds*. 1993; 198(1-2): 51-53. Available from: https://doi.org/10.1016/0925-8388(93)90143-B.

[9] Pei Z, Su Q, Zhang J. Luminescence of Bi^{3+} and the energy transfer from Bi^{3+} to R^{3+} (R = Eu, Dy, Sm, Tb) in alkaline-earth borates. *Solid State Communications*. 1993; 86(6): 377-380. Available from: https://doi.org/10.1016/0038-1098(93)90861-G.

[10] Schubert DM, Alam F, Visi MZ, Knobler CB. Structural characterization and chemistry of the industrially important zinc borate, $Zn[B_3O_4(OH)_3]$. *Chemistry of Materials*. 2003; 15: 866-871. Available from: https://doi.org/10.1021/cm020791z.

[11] Joseph TA, Chopra V, Dhoble SJ. Thermoluminescence studies of zinc borate (ZnB_2O_4) phosphor doped with rare earths for dosimetric aspects. *Luminescence*. 2023; 38(9): 1597-1606. Available from: https://doi.org/10.1002/bio.4542.

[12] Zheng Y, Qu Y, Tian Y, Rong C, Wang Z, Li S, et al. Effect of Eu^{3+}-doped on the luminescence properties of zinc borate nanoparticles. *Colloids and Surfaces A: Physicochemical and Engineering Aspects*. 2009; 349(1-3): 19-22. Available from: https://doi.org/10.1016/j.colsurfa.2009.07.039.

[13] Bulcar K, Kucuk N, Topaksu M, Can N. Thermoluminescence spectra of Tm doped ZnB_2O_4 phosphor prepared via a wet-chemical synthesis. *Applied Radiation and Isotopes*. 2019; 147: 177-181. Available from: https://doi.org/10.1016/j.apradiso.2019.03.016.

[14] Kucuk N, Bulcar K, Dogan T, Garcia Guinea J, Portakal ZG, Karabulut Y, et al. Doping Sm^{3+} into ZnB_2O_4 phosphors and their structural and cathodoluminescence properties. *Journal of Alloys and Compounds*. 2018; 748: 245-251. Available from: https://doi.org/10.1016/j.jallcom.2018.03.153.

[15] Dogan T, Tormo L, Akca S, Kucuk N, Guinea JG, Karabulut Y, et al. Cathodoluminescence and thermoluminescence of ZnB_2O_4:Eu^{3+} phosphors prepared via wet-chemical synthesis. *Ceramics International*. 2019; 45(4): 4918-4925. Available from: https://doi.org/10.1016/j.ceramint.2018.11.191.

[16] Sharma R, Mehta M, Bhargavi GN. Thermoluminescence properties of borate based phosphors: a review. *International Journal of Engineering Research & Technology (IJERT)*. 2023; 12(01): 71-86. Available from: https://doi.org/10.17577/IJERTV12IS010047.

[17] Akça S. Determination of thermoluminescence properties of ZnB_2O_4:Tm^{3+}, Li^+ for dosimetric purposes. *Applied Radiation and Isotopes*. 2020; 157: 109041. Available from: https://doi.org/10.1016/j.apradiso.2020.109041.

[18] Aboud H, Wagiran H, Hussin R. Mechanism of thermoluminescence. *International Journal of Scientific & Engineering Research*. 2012; 3(10): 1-16.

[19] Nambi KS, Bapat VN, Ganguly AK. Thermoluminescence of $CaSO_4$ doped with rare earths. *Journal of Physics C: Solid State Physics*. 1974; 7: 4403. Available from: https://doi.org/10.1088/0022-3719/7/23/027.

[20] Chen R, Lawless JL, Pagonis V. A model for explaining the concentration quenching of thermoluminescence. *Radiation Measurements*. 2011; 46(12): 1380-1384. Available from: https://doi.org/10.1016/j.radmeas.2011.01.022.

[21] Brahme N, Gupta A, Bisen DP, Kher RS, Dhoble SJ. Thermoluminescence and mechanoluminescence of Eu doped Y_2O_3 nanophosphors. *Physics Procedia*. 2009; 29: 97-103. Available from: https://doi.org/10.1016/j.phpro.2012.03.698.

[22] Chen R. On the calculation of activation energies and frequency factors from glow curves. *Journal of Applied Physics*. 1969; 40: 570-585. Available from: https://doi.org/10.1063/1.1657437.

[23] Strauss L. *Review of methods for the determination of the Kinetic parameters of thermoluminescence dosimeters*. Project Thesis. 2007.

[24] Chepyga LM, Hertle E, Ali A, Zigan L, Osvet A, Brabec CJ, et al. Synthesis and photoluminescent properties of the Dy^{3+} doped YSO as a high-temperature thermographic phosphor. *Journal of Luminescence*. 2018; 197: 23-30. Available from: https://doi.org/10.1016/j.jlumin.2017.12.072.